THE JOURNAL OF PHYSICAL CHEMISTRY LETTERS
A JOURNAL OF THE AMERICAN CHEMICAL SOCIETY

pubs.acs.org/JPCL

Letter

Symmetry Breaking: A Classic Example of Quantum Interference Captured by Mixed Quantum/Classical Theory

Kayla Imanzi,[†] Dulat Bostan,[†] Max McCrea, Josh Featherstone, Mark Brouard, and Dmitri Babikov*

Cite This: *J. Phys. Chem. Lett.* 2023, 14, 10617−10623

Read Online

ACCESS | Metrics & More | Article Recommendations

ABSTRACT: The phenomena of propensity and inverse propensity are explored using time-dependent mixed quantum classical theory, MQCT, in which the rotational motion of the molecule is treated quantum mechanically, whereas the scattering process is described classically. Good agreement with the results of accurate full-quantum calculations is reported for a closed shell approximation to the NO + Ar system. It is shown that MQCT reproduces both phenomena in a broad range of the final states of the molecule and for various initial rotational states, offering a unique time-dependent insight. It permits seeing that both propensity and inverse propensity occur due to efficient depopulation of some states at the early postcollisional stage of the scattering process, when the molecule exists in a coherent superposition of many excited states that span a very broad range of angular momentum quantum numbers, populated by an efficient stepladder process of many consecutive transitions with small Δj.

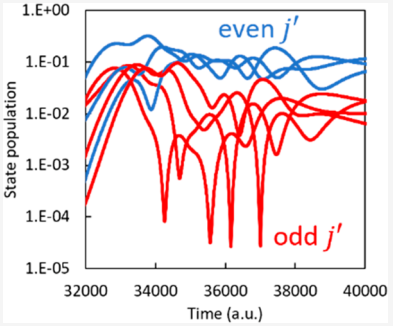

One of the fundamental consequences of a quantum mechanical description of inelastic molecular collisions is the presence of allowed and forbidden state-to-state transitions.[1] One classic example of this sort is a collision of a closed-shell diatomic molecule with an atom. If the molecule is homonuclear, transitions are allowed only between the pairs of rotational states that are characterized by *even* values of Δj, where j is the angular momentum quantum number associated with molecular rotation.[1] For example, if the molecule is initially in the ground state $j = 0$, then only the states with $j' = 2, 4, 6$, *etc.* can be excited in a collision event (we use prime to indicate the final states). Other state-to-state transitions (with *odd* values of Δj) are strictly forbidden. This quantum effect is rooted in the symmetries of rotational wave functions[2,3] and therefore cannot be described by the popular method of classical trajectories (often called a quasi-classical trajectory method)[4,5] which erroneously predicts that a molecule−atom collision leads to a continuous and smooth distribution of rotational angular momentum states,[6−8] with no difference between even and odd values of j.

In order to mimic the quantization of states, classical trajectories are binned into "boxes" associated with different values of j and, in order to mimic the quantum-mechanical selection rules, one popular trick is to make these boxes twice as wide in the case of homonuclear diatomic molecules (to associate all trajectories with allowed transitions only, those with even Δj). While this simple fix may look appropriate for perfectly symmetric diatomic molecules, its deficiency becomes obvious in several important cases of symmetry breaking.[9−12] Namely, if the molecule is heteronuclear, the transitions with odd Δj values become allowed, but usually they remain weaker than those with even Δj. One example of this sort is brought about by isotopic substitutions,[13,14] when the molecule−atom interaction potential remains symmetric but the center of mass of the molecule is slightly shifted. Since isotopes have very similar masses, this shift is typically small, and the transitions with odd Δj remain relatively weak. Another example is when the two atoms in the molecule have similar masses, such as in CO[15−17] or NO diatomics.[5,18,19] In all these cases there is a strong *propensity* toward even Δj values, often called a weak selection rule, but the amount of this propensity differs from one molecule to another and is hard to predict *a priori*, making the binning of classical trajectories into boxes unreliable.

Moreover, as was demonstrated in a classic paper by McCurdy and Miller,[9] for the molecule−atom interaction potentials that possess certain properties, the usual propensity toward even Δj values (seen at smaller values of Δj) may turn into an *inverse propensity* toward odd values of Δj in the range of larger Δj. Clearly, this phenomenon would not be possible to describe by the binning of classical trajectories into any kind of boxes. Importantly, McCurdy and Miller demonstrated that the propensity itself, and the phenomenon of propensity inversion, both originate in the quantum interference effect.[9,20,21] Using the method of classical S-matrix theory

Received: October 17, 2023
Revised: November 16, 2023
Accepted: November 17, 2023
Published: November 20, 2023

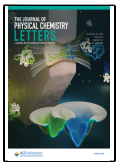

https://doi.org/10.1021/acs.jpclett.3c02887
J. Phys. Chem. Lett. 2023, 14, 10617−10623

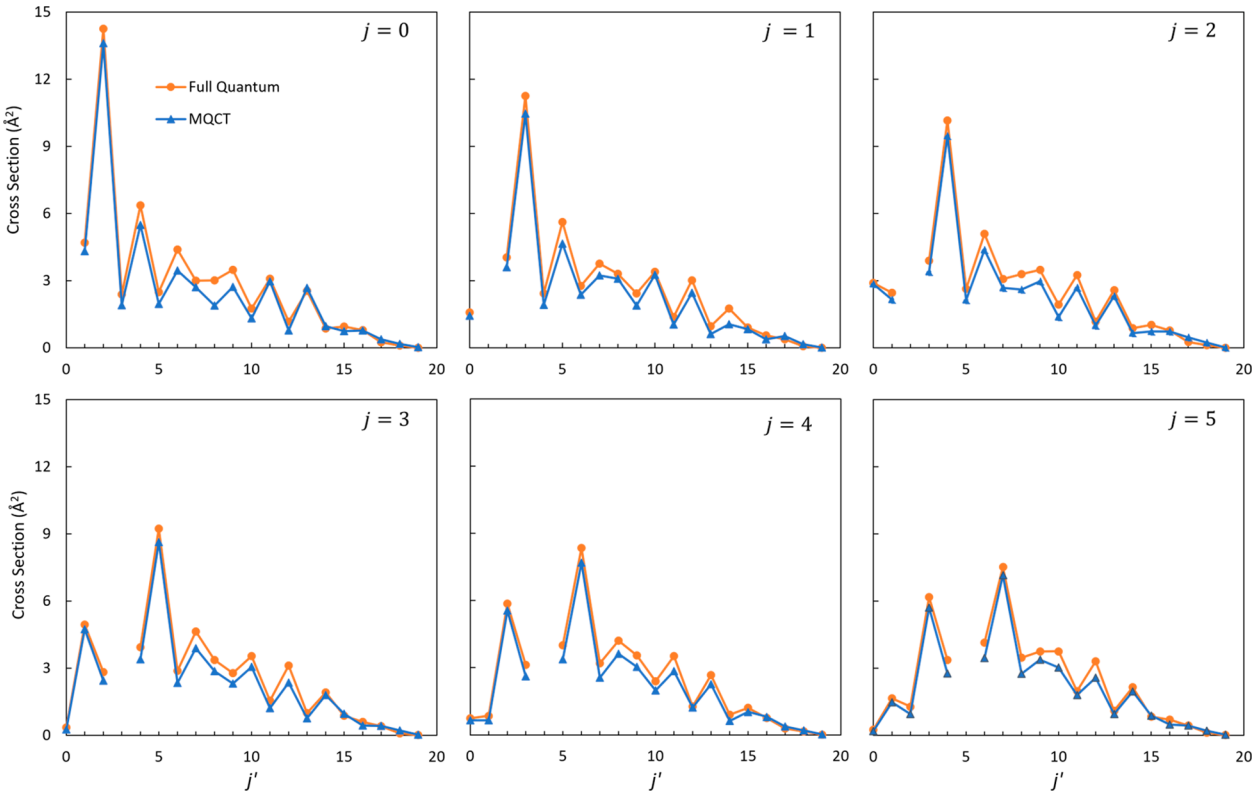

Figure 1. Comparison of inelastic state-to-state transition cross sections for NO + Ar computed by two different methods: MQCT data are blue; HIBRIDON data are orange. Different frames correspond to different initial states of the NO, as indicated in each frame. Various final states are indicated along the horizontal axis. The values of elastic scattering cross sections are much larger and therefore are not included here.

they showed that the interference between different scattering paths with appropriately computed phases leads to constructive (in the case of even Δj) and destructive (in the case of odd Δj) interferences, yielding a strict selection rule in the case of homonuclear molecules, and a weak selection rule in the case of slightly asymmetric molecules, when the destructive interference is not perfect.

More recently, the approach of McCurdy and Miller was employed to explain quantum interference effects observed in the experimentally measured differential cross sections.[18,22] The beauty of their approach is that it allows the rationalization of observations using the interference between a small number of scattering paths (in fact, just four). Unfortunately, this simple framework does not permit the reproduction of the absolute values of the inelastic scattering cross sections. Moreover, the classical *S*-matrix theory of Miller involves an expensive root search, which becomes numerically challenging in the case of molecule−molecule scattering where the number of rotational degrees of freedom becomes large. Of course, full quantum scattering calculations are expected to reproduce the interference effects discussed above, but the issue of computational cost would be even more acute. Namely, for the molecule−molecule systems, such as diatom + symmetric top, or diatom + asymmetric top, the cost of full-quantum calculations is very substantial, particularly at higher collision energies and when the diatom is heavier than H_2.[23−27]

In this Letter we explore an alternative approach for the description of quantum effects in molecular collisions, named the mixed quantum/classical theory (MQCT).[28−35] In our method the scattering process of collision partners (their translational motion) is described approximately using the mean-field Ehrenfest method,[36−39] while the rotational motion of collision partners is described rigorously by solving the time-dependent Schrodinger equation, which incorporates all quantum phenomena associated with their internal states. During the past decade MQCT was applied to several molecular systems and was found to give results often comparable to the full-quantum results.[32,40,41] One important advantage of MQCT is its affordable numerical cost. At present time this is probably the only method capable of treating the most complex case of asymmetric-top-rotor + asymmetric-top-rotor inelastic collision, such as H_2O + H_2O.[42−44] In what follows, we demonstrate that MQCT captures rather accurately the weak selection rules discussed above and gives a reliable description of the propensity inversion, the classic effect of quantum interference described by McCurdy and Miller.

In this study we focus on the NO + Ar system described in a simplified way, with fine structure of the molecule neglected, the rotational states labeled by integer values of j (as if it would be a closed-shell system), and one potential energy surface employed to describe the interaction of NO with Ar atom (half-sum of the A' and A'' states, see ref 19). The propensity properties of this system are well documented.[21,45] This PES describes NO as a rigid rotor, and we follow the same approximation in the calculation of the collision dynamics, keeping the bond length fixed at r = 2.17464 Bohr. This approximation is expected to work well for moderate rotational excitations and collision energies considered in this work.

In MQCT calculations, the rotational wave function of the molecule is represented by the expansion over the basis set of rotational eigenstates. For NO we used a basis set of 20 rotational levels ($0 \leq j \leq 19$) with all associated projection

https://doi.org/10.1021/acs.jpclett.3c02887
J. Phys. Chem. Lett. 2023, 14, 10617−10623

states ($-j \le m \le +j$), or 400 states overall in the rotational basis set. The rotational constant of the NO molecule is B_e = 1.69611 cm^{-1}. Matrix elements for state-to-state transitions were computed on a grid of 81 equally spaced points that covers the molecule−atom distances in the range $4 \le R \le 20$ Bohr. Integration over the polar angle was done by using the Gauss−Legendre quadrature with 40 points. The maximum impact parameter b_{max} = 20 Bohr was chosen that corresponds to the molecule−atom orbital angular momentum quantum number in the range $262 \le l_{max} \le 273$ for the collision energies in the range $600 \le E_{coll} \le 651$ cm^{-1} considered here. One trajectory was initiated for each set of the initial quantum numbers j, $|m|$, and l, or about 270 trajectories with different values of l for each initial state of NO with quantum numbers j and m. The equations of motion were propagated using the fourth-order Runge−Kutta method with constant step-size Δt = 10 au. Other details of MQCT theory, including all equations, can be found in our recent papers.[23,29,33,46]

In order to gauge the accuracy of MQCT we also carried out a set of benchmark full-quantum calculations using the HIBRIDON package[47] with the same simplifying assumptions about the NO + Ar potential energy surface and the same rotational basis set, at one value of total energy E_{tot} = 651 cm^{-1} with maximum value of $J_{tot} \le 190$. A comparison of cross sections obtained by the two methods is presented in Figure 1 for six different initial states of the NO molecule with the corresponding collision energies. From this figure one can see that agreement between the two methods is very good, without any empirical adjustments. For the initial state j = 0 one can see a very pronounced weak selection rule in the range of small Δj values, up to the final j' = 7. Namely, the values of cross sections for even Δj transitions (j' = 2, 4, 6) are much larger than those for odd Δj transitions (j' = 1, 3, 5, 7), producing "zigzag" structure in the dependence of cross section (i.e., oscillations in integral cross sections versus j'). Similar zigzags are seen in all frames of Figure 1, although for the excited rotational states the range of Δj becomes somewhat shorter (i.e., only two zigzags for the initial j = 4 and j = 5 versus three zigzags for the initial j = 0 and j = 1) and appear on both sides of the elastic channel (i.e., not only for the excitation with positive Δj, but also on the quenching side with negative Δj values). This is very clear in the case of initial state j = 5. All of these properties are reliably reproduced by MQCT calculations, as gauged by comparison with HIBRIDON. On average, over all inelastic transitions included in Figure 1, MQCT cross sections are 16% smaller than those from the full quantum calculations, with absolute RMSD of only ~0.47 Å^2.

One can also notice that the normal propensity toward even Δj transitions weakens as Δj is raised (which is seen as a reduction of zigzag amplitude) and eventually vanishes at some point. Namely, for the initial states j = 0, 1, 2 the propensity vanishes near the final j' = 8, for the initial states j = 3, 4 it vanishes near the final j' = 9, and for the initial state j = 5 it vanishes near the final j' = 10, yielding to the *inverse propensity* at higher values of j'. This inverse propensity is very clear in all frames of Figure 1, with *larger* cross sections observed for *odd* Δj and *smaller* cross sections for *even* Δj transitions in the intermediate range of Δj values. Finally, the inverse propensity also weakens and vanishes at some point (near the final j' = 15 or 16, depending on the initial state). Again, all of these properties are accurately captured by MQCT.

McCurdy and Miller[9] explained this behavior by the interplay between dipole (λ = 1) and quadrupole (λ = 2) terms of the molecule + atom interaction potential. Our results are entirely consistent with their explanation, except that in our case, an accurate potential energy surface is employed, represented by a nine-term expansion up to λ = 8. As a numerical experiment, we tried to repeat MQCT calculations for NO + Ar with all odd λ terms removed, keeping only even expansion terms λ = 0, 2, 6, and 8. This, effectively, makes the potential energy surface symmetric, as if the NO were a homonuclear molecule. The result is presented in Figure 2 for

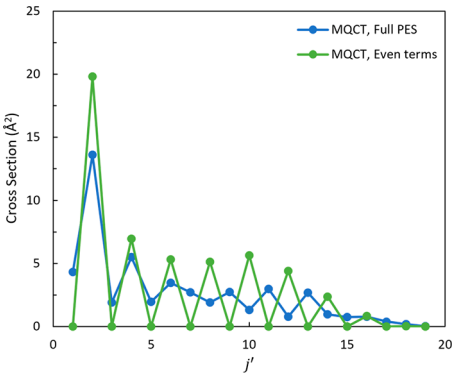

Figure 2. Effect of odd terms of PES expansion on inelastic state-to-state transition cross sections obtained by MQCT calculations for NO + Ar. The data obtained with both even and odd terms included in the PES expansion are shown in blue (full PES, the same data as those in Figure 1). The data obtained without odd terms (even terms only) are shown in green. MQCT method is used in both cases. The initial state was j = 0. Various final states are indicated along the horizontal axis.

the initial j = 0, where we see that propensity (a weak selection rule) is now replaced by a strict selection rule with cross sections being exactly zero for all transitions with odd Δj, just like in the case of a homonuclear diatomic molecule, such as O_2 or N_2. This behavior persists through a wide range of Δj values, without inverse propensity coming into play at all, until the point where cross sections become small (near j' = 15).

The explanation of the oscillations in integral cross section with Δj offered by McCurdy and Miller involved quantum interference between trajectories scattered by different molecular orientations.[9] It is important to note that our approach does not allow for a similar interpretation simply because in the MQCT method different orientations of the molecule with respect to the impinging atomic projectile are described by a wave function that captures all possible orientations at once. Therefore, the aforementioned interference happens between different parts of the MQCT wave function within a matrix element, rather than between different trajectories. Consequently, in MQCT the effect of propensity comes from the matrix elements of potential coupling for state-to-state transitions, computed using the wave functions of the individual quantum states. In Figure 3 we present MQCT matrix elements for the excitation of various final rotational states of the NO molecule starting from the initial state j = 0. Looking at these pictures one should keep in mind that at the collision energy considered here ($E_{coll} \approx 600$ cm^{-1}) scattering partners can explore only the range of $R > 6$ bohr. This follows from the diagonal matrix element $0 \rightarrow 0$ shown in red in Figure 3. From Figure 3 we can clearly see that, through the entire range of molecule−atom distances, the matrix element responsible for the $0 \rightarrow 2$ transition is much larger than those for $0 \rightarrow 1$ and $0 \rightarrow 3$ transitions, which explains the first

https://doi.org/10.1021/acs.jpclett.3c02887
J. Phys. Chem. Lett. 2023, 14, 10617−10623

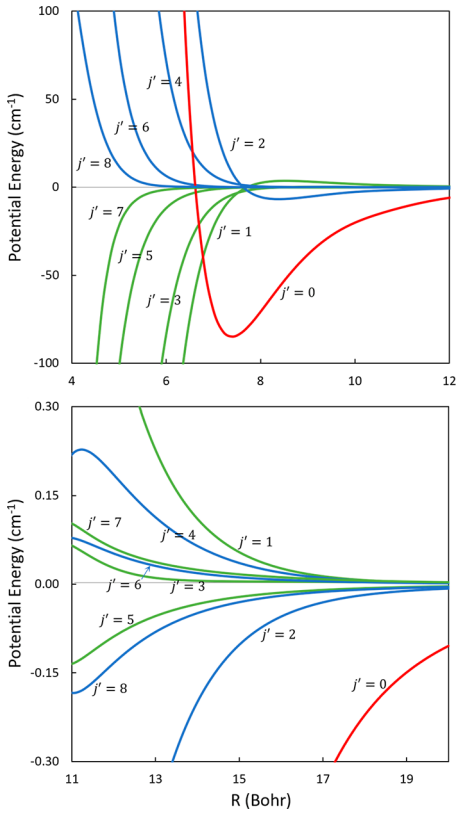

Figure 3. Radial dependence of state-to-state transition matrix elements in MQCT method, for rotational excitations in NO + Ar collision, starting from the ground state $j = 0$. Upper frame emphasizes a short-range part of the interaction potential with stronger interaction. Lower frame is focused on a long-range weak-interaction part of the process. The diagonal matrix element responsible for elastic scattering is shown in red, while blue and green colors are used for even and odd Δj transitions, respectively.

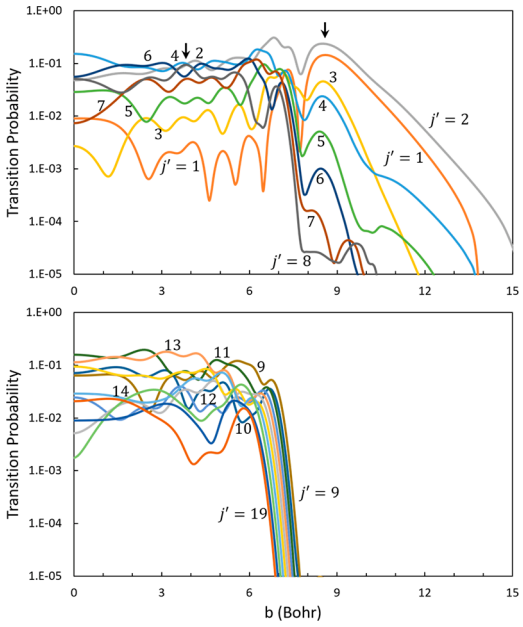

Figure 4. Dependence of state-to-state transition probabilities on collision impact parameter in MQCT calculations for rotational excitations in a NO + Ar collision. Upper frame emphasizes excitation of the first eight states. Lower frame is for higher energy states. The initial state is $j = 0$. Final states are labeled by numbers and are color coded for convenience. Small arrows indicate two values of the impact parameter considered in Figure 5.

(largest) zigzag in Figure 2. Next, we can see that in the long-range part of the interaction (lower frame of Figure 3) the matrix element for the $0 \rightarrow 4$ transition is larger than that for $0 \rightarrow 3$, which explains the second (smaller) zigzag in Figure 2. But it is hard to claim that all matrix elements for transitions with even Δj are larger than those for transitions with odd Δj. In particular, the matrix element for $0 \rightarrow 6$ transition is smaller than those for $0 \rightarrow 5$ and $0 \rightarrow 7$, which means that in order to explain the oscillations beyond $j' = 4$ we must invoke something else.

Before we discuss this "something else", it is instructive to analyze the contributions of individual partial waves to the state-to-state transition process. In MQCT partial waves correspond to different values of molecule−atom orbital angular momentum l that correlates with collision impact parameter b. In Figure 4 we present the dependence of state-to-state transition probabilities on collision impact parameter up to $b = 15$ Bohr, starting from the initial state $j = 0$. Excitation of the first eight states is shown in the upper frame, while the excitation of states with $j' = 9$ and above is shown in the lower frame of Figure 4. We see first that excitations of the lower j' states occur in a way rather different from those for upper j' states. Namely, for excitation of $j' = 1$, 2, and 3 the collisions with large values of impact parameter, $b \approx 8$ Bohr and above, make very significant contributions (see upper frame of Figure 4). Such collisions correspond to *glancing* trajectories that pass through the asymptotic range of the molecule−atom PES, without a strong encounter. These glancing trajectories also contribute some to the excitation of $j' = 4$, 5 and 6, but they can be barely identified in the dependencies for $j' = 7$ and 8 and are entirely absent in the excitation of $j' = 9$ and higher states (shown in the lower frame of Figure 4).

In contrast, for the excitations of $j' \geq 9$ only the trajectories with small impact parameters $b < 8$ Bohr are found to contribute (see lower frame in Figure 4). These *impulsive* trajectories correspond to strong encounters. Indeed, from Figure 4 we see that in the range $b < 8$ Bohr all transition probabilities slightly oscillate but remain relatively high, in the range of values determined by a head-on collision with $b = 0$. The conclusion is that glancing trajectories are efficient only for transitions with low Δj, while the impulsive trajectories can drive all transitions, including those with high Δj.

Manifestation of the weak selection rule (the normal propensity) is very clear in the top frame of Figure 4. In the inner range of impact parameter ($b < 8$ Bohr) it shows that transition probabilities for excitation of $j' = 2$, 4, and 6 are systematically larger than those for excitation of $j' = 1$, 3, 5 and 7, which corresponds to three zigzags in Figure 2. In the outer range ($b > 8$ Bohr) it shows that the transition probably for $j' = 2$ dominates over those for excitation of $j' = 1$ and 3, but for $j' = 4$ and higher, it decreases monotonically, without any obvious propensity. Therefore, we conclude that the major source of propensity is in the impulsive trajectories with small impact parameters.[48,49] Glancing trajectories make significant contributions to the first zigzag in Figure 2 (small Δj values), but they have minor influence on the following zigzags (second, third, etc.), and no influence at all on the inverse propensity at higher Δj. The inverse propensity manifests clearly in the lower frame of Figure 4, where we see that in the

https://doi.org/10.1021/acs.jpclett.3c02887
J. Phys. Chem. Lett. 2023, 14, 10617−10623

inner range of impact parameter (b < 8 Bohr) transition probabilities for excitation of odd j' = 9, 11, and 13 are systematically larger than those for excitation of j' = 10, 12 and 14, which is consistent with three inverse zigzags in the range 9 ≤ j' ≤ 14 in Figure 2 (and similar in all frames of Figure 1).

At this point, one should raise the question of how the states in the range j' = 9 and above are excited (starting from j = 0). Matrix elements for the excitation of these states directly from the ground state are negligibly small, but the values of cross sections in the range of 9 ≤ j' ≤ 14 in Figure 2 are comparable to those in the range of 3 ≤ j' ≤ 8. This means that the mechanism of transitions with large Δj is efficient and different from transitions occurring directly from the ground state j = 0.

In order to obtain more insight into the excitation of higher j' states, we plotted the time dependence of the state populations for two typical MQCT trajectories, one with impact parameter b = 3.7 Bohr (small value in the inner range) and the other with b = 8.3 Bohr (large value in the outer range). These can be considered as "slices" through Figure 4, at the spots indicated by two small arrows in the upper frame of that figure. Also, in these calculations for two individual trajectories, we neglected the Coriolis coupling terms that tend to "smooth" some features of the potential coupling discussed below (although the Coriolis coupling by itself is not responsible for any critical effect). The results are shown in Figure 5. Note that in MQCT each trajectory, in principle, can contribute to transitions into all states included in the rotational basis set, but the result of collision depends on the collision impact parameter.

The upper frame of Figure 5 corresponds to a glancing trajectory. Populations of states with 1 ≤ j' ≤ 8 grow rather monotonically during a relatively long interval of time (which, in fact, extends beyond the figure frame) without a well-defined instant of strong encounter. As discussed above, this trajectory makes some contribution to the first zigzag in Figure 2. Indeed, in the upper frame of Figure 5 we see clearly that the population of the state j' = 2 exceeds those of states j' = 1 and 3 at all times. However, the populations of other even states (e.g., j' = 4 and 6) remain relatively small and therefore cannot contribute much to the propensity observed in the total cross sections. This, again, agrees with the results presented in Figure 4 above.

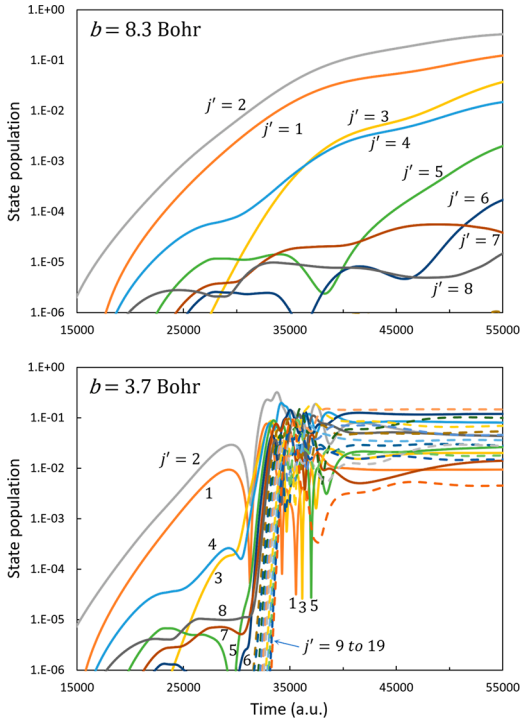

Figure 5. Time dependence of state populations for two typical MQCT trajectories with indicated values of impact parameter during NO + Ar collision. The initial state is j = 0. Final states are labeled by numbers and are color coded for convenience. Dashed lines are used for rotational states with j' ≥ 9.

In contrast, the lower frame of Figure 5 clearly shows the process of a short and strong encounter between the collision partners that happens near t ≈ 35000 au. At the precollisional stage, t < 30000 au, the time evolution of state populations is similar to that of a glancing trajectory (in the upper frame of Figure 5). Namely, populations of states 1 ≤ j' ≤ 8 increase rather monotonically, with j' = 2 and 1 dominating over the other states. But at the beginning of the encounter, near t ≈ 31000 au, the populations of states j' = 2 and 1 drop sharply, transferring their populations to another pair of states (j' = 4 and 3) that grow very quickly and synchronously with the decrease of state populations in j' = 2 and 1. Soon after that, the next pair of states starts gaining populations quickly (j' = 6 and 5) and then the next pair (j' = 8 and 7). As for selection rules, we can see that although the state j' = 2 clearly dominates in this process, the propensity for j' = 4 and 6 is not at all clear during the precollisional stage. The populations of j' = 4 and 6 change over time and sometimes are larger but sometimes are smaller than the populations of their neighbors with odd j' = 3, 5, and 7. However, it becomes rather clear that the rotational excitation process works in a *stepladder* fashion that consists of many consecutive transitions with small values of Δj, rather than one direct process of excitation of all states, including those with large Δj values. The ability to observe this phenomenon is a very important advantage of our MQCT method, which, being a time-dependent approach, permits us to see the time evolution of state populations during the collision process.

Going back to the lower frame of Figure 5, we see that as the collision progresses, more and more upper states get involved. Thus, the states with 9 ≤ j' ≤ 19 (that have negligible direct transitions from j = 0) start receiving populations from their neighbors and come into play quickly during a short time interval between t ≈ 32000 and 34000 au. Near the middle of the collision event, we observe a superposition of all states included in the basis with populations oscillating between 0.005 and 0.1, with no obvious propensity. However, a very interesting phenomenon can be observed shortly after that. Namely, at the early postcollisional stage, between t ≈ 35000 and 36000 au, the populations of odd states j' = 1, 3, and 5 drop sharply by several orders of magnitude (down to ~10^{-5}, see lower frame of Figure 5 and the image in the Abstract) and, although these states partially recover their populations later, they remain small compared to populations of their neighbors with even values of j', and this is exactly what gives rise to the propensity (and the weak selection rule). Moreover, a careful inspection of time dependencies in the lower frame of Figure 5 indicates that the inverse propensity for the states in the range 9 ≤ j' ≤ 14 is also established during the early postcollisional stage by more efficient depopulation of states j' = 10, 12 and 14.

https://doi.org/10.1021/acs.jpclett.3c02887
J. Phys. Chem. Lett. 2023, 14, 10617−10623

To conclude, it appears that the origin of the propensity and inverse propensity is *not* in an efficient population of some states in the molecule, with some other states remaining unpopulated spectators. Instead, both propensity and inverse propensity occur due to efficient *depopulation* of some states right after the collision, when the molecule exists in a coherent superposition of many excited states that span a very broad range of angular momentum quantum numbers (basically, all states accessible at a given collision energy). The ensemble of these states is populated by an efficient stepladder process of consecutive transitions with small values of Δj that takes place along the impulsive trajectories launched with small impact parameters and thus able to penetrate deeper into the interaction region.[48,49] It is perhaps worth noting that similar symmetry breaking behavior has been observed and reproduced by MQCT for isotopically substituted S_2 + Ar[14] and for CO + H, which will be subject to a separate forthcoming paper.

This interesting story can be revealed only by a time-dependent scattering method, such as our mixed quantum-classical theory, MQCT. It is shown that MQCT reproduces both propensity and inverse propensity in a broad range of the final states of the molecule and for various initial rotational states, with the accuracy of predicted state-to-state cross sections on the order of 15% (relative to accurate full-quantum time-independent calculations). This theory method remains computationally affordable for larger molecules, which opens new opportunities for the exploration of more complicated molecular systems. Moreover, since MQCT carries phase information and describes the coherent superposition of rotational states, it has potential for the prediction of stereodynamical properties, such as polarization-dependent differential cross sections and alignment moments.[50−52]

AUTHOR INFORMATION

Corresponding Author

Dmitri Babikov − *Chemistry Department, Marquette University, Milwaukee, Wisconsin 53201-1881, United States;* orcid.org/0000-0002-4667-7645; Email: dmitri.babikov@mu.edu

Authors

Kayla Imanzi − *Chemistry Department, Marquette University, Milwaukee, Wisconsin 53201-1881, United States*

Dulat Bostan − *Chemistry Department, Marquette University, Milwaukee, Wisconsin 53201-1881, United States;* orcid.org/0009-0007-2504-1027

Max McCrea − *Chemistry Research Laboratory, Department of Chemistry, University of Oxford, Oxford OX1 3TA, U.K.*

Josh Featherstone − *Chemistry Research Laboratory, Department of Chemistry, University of Oxford, Oxford OX1 3TA, U.K.*

Mark Brouard − *Chemistry Research Laboratory, Department of Chemistry, University of Oxford, Oxford OX1 3TA, U.K.;* orcid.org/0000-0003-3421-0850

Complete contact information is available at: https://pubs.acs.org/10.1021/acs.jpclett.3c02887

Author Contributions

†K.I. and D.B. contributed equally to this work.

Notes

The authors declare no competing financial interest.

ACKNOWLEDGMENTS

This research was supported by NASA Astrophysics Research and Analysis program, grant number 80NSSC24K0208. D. Babikov acknowledges the support of Way Klingler Research Fellowship and of the Pfletschinger-Habermann Research Fund. K. Imanzi acknowledges the support of undergraduate chemistry summer research program at Marquette and the E&R Lafferty Scholarship. D. Bostan acknowledges the support of Eisch Fellowship and the Bournique Memorial Fellowship. M. Brouard, J. Featherstone, and M. McCrea thank the EPSRC for financial support (via Program Grant EP/T021675/1). We used resources of the National Energy Research Scientific Computing Center, which is supported by the Office of Science of the U.S. Department of Energy under Contract No. DE-AC02-5CH11231. This research also used HPC resources at Marquette, funded in part by the National Science foundation award CNS-1828649.

REFERENCES

(1) Demtröder, W. *Molecular Physics: Theoretical Principles and Experimental Methods*; John Wiley & Sons: Weinheim, Germany, 2005.

(2) Bunker, P. R.; Jensen, P. *Molecular Symmetry and Spectroscopy*; NRC Research Press: Ottawa, Canada, 2006; Vol. *46853*.

(3) Bunker, P. R.; Papoušek, D. The Symmetry Groups of Linear Molecules. *J. Mol. Spectrosc.* **1969**, *32* (3), 419−429.

(4) Aoiz, F. J.; Verdasco, J. E.; Herrero, V. J.; Sáez Rábanos, V.; Alexander, M. A. Attractive and Repulsive Interactions in the Inelastic Scattering of NO by Ar: A Comparison between Classical Trajectory and Close-Coupling Quantum Mechanical Results. *J. Chem. Phys.* **2003**, *119* (12), 5860−5866.

(5) Nichols, B.; Chadwick, H.; Gordon, S. D. S.; Eyles, C. J.; Hornung, B.; Brouard, M.; Alexander, M. H.; Aoiz, F. J.; Gijsbertsen, A.; Stolte, S. Steric Effects and Quantum Interference in the Inelastic Scattering of NO (X)+ Ar. *Chem. Sci.* **2015**, *6* (4), 2202−2210.

(6) Fleurat-Lessard, P.; Grebenshchikov, S. Y.; Siebert, R.; Schinke, R.; Halberstadt, N. Theoretical Investigation of the Temperature Dependence of the O+ O_2 Exchange Reaction. *J. Chem. Phys.* **2003**, *118* (2), 610−621.

(7) McBane, G. C.; Nguyen, L. T.; Schinke, R. Photodissociation of Ozone in the Hartley Band: Product State and Angular Distributions. *J. Chem. Phys.* **2010**, *133* (14), 4312.

(8) Warter, M. L.; Gunthardt, C. E.; Wei, W.; McBane, G. C.; North, S. W. Nascent O_2 ($a^1\Delta_g$, v= 0, 1) Rotational Distributions from the Photodissociation of Jet-Cooled O_3 in the Hartley Band. *J. Chem. Phys.* **2018**, *149* (13), 4309.

(9) McCurdy, C. W.; Miller, W. H. Interference Effects in Rotational State Distributions: Propensity and Inverse Propensity. *J. Chem. Phys.* **1977**, *67* (2), 463−468.

(10) Babikov, D.; Walker, R. B.; T Pack, R. A Quantum Symmetry Preserving Semiclassical Method. *J. Chem. Phys.* **2002**, *117* (19), 8613−8622.

(11) Gijsbertsen, A.; Linnartz, H.; Taatjes, C. A.; Stolte, S. Quantum Interference as the Source of Steric Asymmetry and Parity Propensity Rules in NO- Rare Gas Inelastic Scattering. *J. Am. Chem. Soc.* **2006**, *128* (27), 8777−8789.

(12) Kłos, J.; Aoiz, F. J.; Menéndez, M.; Brouard, M.; Chadwick, H.; Eyles, C. J. Ab Initio Studies of the Interaction Potential for the Xe−NO ($X^2\Pi$) van Der Waals Complex: Bound States and Fully Quantum and Quasi-Classical Scattering. *J. Chem. Phys.* **2012**, *137* (1), 4305.

(13) Bop, C. T.; Quintas-Sánchez, E.; Sur, S.; Robin, M.; Lique, F.; Dawes, R. Inelastic Scattering in Isotopologues of O_2−Ar: The Effects of Mass, Symmetry, and Density of States. *Phys. Chem. Chem. Phys.* **2021**, *23* (10), 5945−5955.

(14) Mandal, B. Development of MQCT Method for Calculations of Collisional Energy Transfer for Astrochemistry and Planetary

Atmospheres. Ph.D. Thesis, Marquette University, Milwaukee, WI, 2021.
(15) Balakrishnan, N.; Yan, M.; Dalgarno, A. Quantum-Mechanical Study of Rotational and Vibrational Transitions in CO Induced by H Atoms. *Astrophys. J.* **2002**, *568* (1), 443.
(16) Shepler, B. C.; Yang, B. H.; Kumar, T. J. D.; Stancil, P. C.; Bowman, J. M.; Balakrishnan, N.; Zhang, P.; Bodo, E.; Dalgarno, A. Low Energy H+ CO Scattering Revisited-CO Rotational Excitation with New Potential Surfaces. *Astron. Astrophys.* **2007**, *475* (2), L15−L18.
(17) Song, L.; van der Avoird, A.; Groenenboom, G. C. Three-Dimensional Ab Initio Potential Energy Surface for H−CO ($\tilde{X}^2A'$). *J. Phys. Chem. A* **2013**, *117* (32), 7571−7579.
(18) Eyles, C. J.; Brouard, M.; Yang, C.-H.; Kłos, J.; Aoiz, F. J.; Gijsbertsen, A.; Wiskerke, A. E.; Stolte, S. Interference Structures in the Differential Cross-Sections for Inelastic Scattering of NO by Ar. *Nat. Chem.* **2011**, *3* (8), 597−602.
(19) Alexander, M. H. A New, Fully Ab Initio Investigation of the NO (X 2Π) Ar System. I. Potential Energy Surfaces and Inelastic Scattering. *J. Chem. Phys.* **1999**, *111* (16), 7426−7434.
(20) Joswig, H.; Andresen, P.; Schinke, R. Electronic Fine Structure Transitions and Rotational Excitation in NO Rare Gas Collisions. *J. Chem. Phys.* **1986**, *85* (4), 1904−1914.
(21) Andresen, P.; Joswig, H.; Pauly, H.; Schinke, R. Resolution of Interference Effects in the Rotational Excitation of NO (N═O) by Ar. *J. Chem. Phys.* **1982**, *77* (4), 2204−2205.
(22) Brouard, M.; Gordon, S. D. S.; Nichols, B.; Walpole, V.; Aoiz, F. J.; Stolte, S. Differential Steric Effects in the Inelastic Scattering of NO (X)+ Ar: Spin−Orbit Changing Transitions. *Phys. Chem. Chem. Phys.* **2019**, *21* (26), 14173−14185.
(23) Semenov, A.; Babikov, D. Mixed Quantum/Classical Calculations of Total and Differential Elastic and Rotationally Inelastic Scattering Cross Sections for Light and Heavy Reduced Masses in a Broad Range of Collision Energies. *J. Chem. Phys.* **2014**, *140* (4), 4306.
(24) Gao, Z.; Loreau, J.; Van Der Avoird, A.; Van De Meerakker, S. Y. T. Direct Observation of Product-Pair Correlations in Rotationally Inelastic Collisions of ND_3 with D_2. *Phys. Chem. Chem. Phys.* **2019**, *21* (26), 14033−14041.
(25) Ndengue, S. A.; Dawes, R.; Gatti, F. Rotational Excitations in CO−CO Collisions at Low Temperature: Time-Independent and Multiconfigurational Time-Dependent Hartree Calculations. *J. Phys. Chem. A* **2015**, *119* (28), 7712−7723.
(26) Żółtowski, M.; Loreau, J.; Lique, F. Collisional Energy Transfer in the CO−CO System. *Phys. Chem. Chem. Phys.* **2022**, *24* (19), 11910−11918.
(27) Joy, C.; Mandal, B.; Bostan, D.; Babikov, D. Mixed Quantum/Classical Theory for Rotational Energy Exchange in Symmetric-Top-Rotor+ Linear-Rotor Collisions and a Case Study of the ND 3+ D 2 System. *Phys. Chem. Chem. Phys.* **2023**, *25*, 17287−17299.
(28) Babikov, D.; Semenov, A. Recent Advances in Development and Applications of the Mixed Quantum/Classical Theory for Inelastic Scattering. *J. Phys. Chem. A* **2016**, *120* (3), 319−331.
(29) Mandal, B.; Semenov, A.; Babikov, D. Calculations of Differential Cross Sections Using Mixed Quantum/Classical Theory of Inelastic Scattering. *J. Phys. Chem. A* **2018**, *122* (30), 6157−6165.
(30) Mandal, B.; Semenov, A.; Babikov, D. Adiabatic Trajectory Approximation within the Framework of Mixed Quantum/Classical Theory. *J. Phys. Chem. A* **2020**, *124* (47), 9877−9888.
(31) Semenov, A.; Mandal, B.; Babikov, D. MQCT: User-Ready Program for Calculations of Inelastic Scattering of Two Molecules. *Comput. Phys. Commun.* **2020**, *252*, No. 107155.
(32) Mandal, B.; Joy, C.; Bostan, D.; Eng, A.; Babikov, D. Adiabatic Trajectory Approximation: A New General Method in the Toolbox of Mixed Quantum/Classical Theory for Collisional Energy Transfer. *J. Phys. Chem. Lett.* **2023**, *14* (3), 817−824.
(33) Bostan, D.; Mandal, B.; Joy, C.; Babikov, D. Description of Quantum Interference Using Mixed Quantum/Classical Theory of Inelastic Scattering. *Phys. Chem. Chem. Phys.* **2023**, *25*, 15683−15692.
(34) Semenov, A.; Babikov, D. Mixed Quantum/Classical Theory of Rotationally and Vibrationally Inelastic Scattering in Space-Fixed and Body-Fixed Reference Frames. *J. Chem. Phys.* **2013**, *139* (17), 4108.
(35) Mandal, B.; Bostan, D.; Joy, C.; Babikov, D. MQCT 2024: A Program for Calculations of Inelastic Scattering of Two Molecules (New Version Announcement). *Comput. Phys. Commun.* **2024**, *294*, 108938.
(36) Billing, G. D. Semiclassical Treatment of Molecular Roto-Vibrational Energy Transfer. *Comput. Phys. Rep.;(Netherlands)* **1984**, *1* (5), 239−296.
(37) Billing, G. D. *The Quantum Classical Theory*; Oxford University Press: New York, USA, 2003.
(38) Coletti, C.; Billing, G. D. Quantum-Classical Calculation of Cross Sections and Rate Constants for the H_2 + CN → HCN + H Reaction. *J. Chem. Phys.* **2000**, *113* (24), 11101−11108.
(39) Hong, Q.; Bartolomei, M.; Esposito, F.; Coletti, C.; Sun, Q.; Pirani, F. Reconciling Experimental and Theoretical Vibrational Deactivation in Low-Energy O + N_2 Collisions. *Phys. Chem. Chem. Phys.* **2021**, *23* (29), 15475−15479.
(40) Semenov, A.; Dubernet, M.-L.; Babikov, D. Mixed Quantum/Classical Theory for Inelastic Scattering of Asymmetric-Top-Rotor+ Atom in the Body-Fixed Reference Frame and Application to the H2O+ He System. *J. Chem. Phys.* **2014**, *141* (11), 4304.
(41) Semenov, A.; Babikov, D. Mixed Quantum/Classical Theory for Molecule−Molecule Inelastic Scattering: Derivations of Equations and Application to N2+ H2 System. *J. Phys. Chem. A* **2015**, *119* (50), 12329−12338.
(42) Semenov, A.; Babikov, D. MQCT. I. Inelastic Scattering of Two Asymmetric-Top Rotors with Application to H_2O+ H_2O. *J. Phys. Chem. A* **2017**, *121* (26), 4855−4867.
(43) Mandal, B.; Babikov, D. Rate Coefficients for Rotational State-to-State Transitions in H_2O+ H_2O Collisions for Cometary and Planetary Applications, as Predicted by Mixed Quantum-Classical Theory. *Astron. Astrophys.* **2023**, *671*, A51.
(44) Mandal, B.; Babikov, D. Improved Temperature Dependence of Rate Coefficients for Rotational State-to-State Transitions in H_2O + H_2O Collisions. *Astron. Astrophys.* **2023**, *678*, A51.
(45) Alexander, M. H. Propensity Rules for Rotationally Inelastic Collisions of Symmetric Top Molecules or Linear Polyatomic Molecules with Structureless Atoms. *J. Chem. Phys.* **1982**, *77* (4), 1855−1865.
(46) Semenov, A.; Babikov, D. Accurate Calculations of Rotationally Inelastic Scattering Cross Sections Using Mixed Quantum/Classical Theory. *J. Phys. Chem. Lett.* **2014**, *5* (2), 275−278.
(47) Alexander, M. H.; Dagdigian, P. J.; Werner, H.-J.; Kłos, J.; Desrousseaux, B.; Raffy, G.; Lique, F. Hibridon: A Program Suite for Time-Independent Non-Reactive Quantum Scattering Calculations. *Comput. Phys. Commun.* **2023**, *289*, No. 108761.
(48) Hornung, B. Rotational Polarisation Effects in the Inelastic Collisions of NO (X) and Ar. Ph.D. Thesis, Oxford University, UK, 2013.
(49) Kłos, J.; Aoiz, F. J.; Verdasco, J. E.; Brouard, M.; Marinakis, S.; Stolte, S. Fully Quantum State-Resolved Inelastic Scattering between He and NO ($X^2\Pi$). *J. Chem. Phys.* **2007**, *127* (3), 1102.
(50) Chadwick, H.; Nichols, B.; Gordon, S. D. S.; Hornung, B.; Squires, E.; Brouard, M.; Kłos, J.; Alexander, M. H.; Aoiz, F. J.; Stolte, S. Inelastic Scattering of NO by Kr: Rotational Polarization over a Rainbow. *J. Phys. Chem. Lett.* **2014**, *5* (19), 3296−3301.
(51) Wang, F.; Lin, J.-S.; Liu, K. How to Measure a Complete Set of Polarization-Dependent Differential Cross Sections in a Scattering Experiment with Aligned Reagents? *J. Chem. Phys.* **2014**, *140* (8), 4202.
(52) Perreault, W. E.; Mukherjee, N.; Zare, R. N. Cold Quantum-Controlled Rotationally Inelastic Scattering of HD with H_2 and D_2 Reveals Collisional Partner Reorientation. *Nat. Chem.* **2018**, *10* (5), 561−567.

https://doi.org/10.1021/acs.jpclett.3c02887
J. Phys. Chem. Lett. 2023, 14, 10617−10623